Microscopic analysis of nuclear quantum phase transitions in the N~90 region

Li, Z. P.; Nikšić, Tamara; Vretenar, Dario; Meng, Jie; Lalazissis, G. A.; Ring, Peter

Microscopic analysis of nuclear quantum phase transitions in the $N \approx 90$ region

Z. P. Li,* T. Nikšić, and D. Vretenar
Physics Department, Faculty of Science, University of Zagreb, Croatia

J. Meng
School of Physics, Peking University, Beijing, People's Republic of China

G. A. Lalazissis
Department of Theoretical Physics, Aristotle University of Thessaloniki, GR-54124, Greece

P. Ring
Physik-Department der Technischen Universität München, D-85748 Garching, Germany
(Received 9 December 2008; revised manuscript received 9 March 2009; published 1 May 2009)

The analysis of shape transitions in Nd isotopes, based on the framework of relativistic energy-density functionals and restricted to axially symmetric shapes in T. Nikšić, D. Vretenar, G. A. Lalazissis, and P. Ring [Phys. Rev. Lett. **99**, 092502 (2007)], is extended to the region $Z = 60, 62, 64$ with $N \approx 90$ and includes both β and γ deformations. Collective excitation spectra and transition probabilities are calculated starting from a five-dimensional Hamiltonian for quadrupole vibrational and rotational degrees of freedom, with parameters determined by constrained self-consistent relativistic mean-field calculations for triaxial shapes. The results reproduce available data and show that there is an abrupt change of structure at $N = 90$ that can be approximately characterized by the X(5) analytic solution at the critical point of the first-order quantum phase transition between spherical and axially deformed shapes.

DOI: 10.1103/PhysRevC.79.054301 PACS number(s): 21.60.Jz, 21.60.Ev, 21.10.Re, 21.90.+f

I. INTRODUCTION

The evolution of shell structures governs the variation of ground-state nuclear shapes along isotopic and isotonic chains. Nuclear structure explores a variety of phenomena related to structural evolution including, for instance, the reduction of spherical shell gaps and modifications of magic numbers in nuclei far from stability, occurrence of islands of inversion and coexistence of shapes with different deformations. As the number of nucleons changes from nucleus to nucleus, in general one observes a gradual evolution of different shapes—spherical, axially deformed, shapes that are soft with respect to triaxial deformations. These shape transitions reflect the underlying modifications of single-nucleon shell structure and interactions between valence nucleons. An especially interesting feature is the possible occurrence of shape phase transitions and critical-point phenomena for particular values of the number of protons and neutrons. Phase transitions in the equilibrium shapes of nuclei correspond to first- and second-order quantum phase transitions (QPT) between competing ground-state phases induced by variation of a nonthermal control parameter (number of nucleons) at zero temperature [1–3].

Nuclear quantum phase transitions have been the subject of extensive experimental and theoretical studies during the past decade. For recent reviews and an exhaustive bibliography we refer the reader to Refs. [4–8]. Even though phase transitions in finite systems can be defined only in the classical limit in which the number of constituents tends to infinity, i.e., the transition is actually smoothed out in finite systems, there are nevertheless clear experimental signatures of abrupt changes in structure properties of finite nuclei with the addition or subtraction of only few nucleons. This is another distinct feature of QPT in atomic nuclei, i.e., the physical control parameter, number of nucleons, can take only discrete integer values. Expectation values of suitably chosen operators, that as observables characterize the state of a nuclear system, can be used as order parameters [9].

Theoretical studies of nuclear QPT are typically based on macroscopic geometric models of nuclear shapes and potentials [8] and/or semimicroscopic algebraic models [7]. In the geometric framework QPTs are analyzed in terms of a Bohr collective Hamiltonian for shape variables and can be related to the concept of critical-point symmetries that provide parameter-independent predictions for excitation spectra and electromagnetic transition rates for nuclei at the phase transition point. Alternatively, in the algebraic approach [e.g., the interacting boson model (IBM)] different shapes coincide with particular dynamical symmetries of some algebraic structure, and the phase transition occurs when these symmetries are broken in a specific way. The two frameworks can be related, for instance, by using the coherent state formalism [10,11] that allows us to establish a correspondence between the symmetry limits of the algebraic Hamiltonian and energy functionals expressed in terms of collective shape variables. In both approaches, geometric and algebraic, the description of QPT is based on model-specific Hamiltonians that by construction describe shape changes.

*School of Physics, Peking University, Beijing, People's Republic of China.

A shape phase transition is then accessed by variation of a control parameter.

The two best-studied classes of nuclear shape phase transitions, both theoretically and experimentally, correspond to a second-order QPT between spherical and γ-soft shapes [12,13] and a first-order QPT between spherical and axially deformed shapes [14,15]. The former is a phase transition in one degree of freedom (the axial deformation β) and, in the IBM language, represents a transition between the U(5) and O(6) dynamical symmetries in the limit of large boson number. The critical point of phase transition can also be related to a dynamical symmetry: in this case E(5) [12], and the experimental realization of this critical-point symmetry was first identified in the spectrum of ^{134}Ba [13]. The second type of shape transitions, between spherical and axially deformed nuclei, is more commonly encountered and involves two degrees of freedom—the deformations β and γ. The critical point of this phase transition, denoted X(5), does not correspond to a dynamical symmetry in the usual sense [14]. Nevertheless, for the particular case in which the β and γ degrees of freedom are decoupled, an approximate analytic solution at the critical point of phase transition can be expressed in terms of zeros of Bessel functions of irrational order [14]. Evidence for the empirical realization of X(5) phase transition was first reported for ^{152}Sm and other $N = 90$ isotones in Ref. [15].

Even though phenomenological approaches to nuclear QPT have been very successful, and the predicted isotopic trends for various observables are in very good agreement with data, it would clearly be desirable to have a fully microscopic description of shape phase transitions, starting from nucleonic degrees of freedom. This is especially important in view of the fact that the physical control parameter in nuclear QPT is the actual number of nucleons in a nucleus, rather than a strength parameter of a model-specific, Ising-type Hamiltonian.

Several recent studies [16–21] have reported microscopic calculations of potential energy surfaces as functions of quadrupole deformation, for a number of isotopic chains in which the occurrence of shape phase transitions had been predicted. Potentials calculated with a constraint on the mass quadrupole moment display shape transitions from spherical to deformed configurations. In Ref. [22] we analyzed shape transitions in Nd isotopes, using a microscopic model based on relativistic energy-density functionals (EDF). Starting from constrained self-consistent mean-field calculations of potential energy curves, the generator coordinate method (GCM) [23] was used to perform configuration mixing of angular-momentum and particle-number projected relativistic wave functions. It was shown that the microscopic framework based on universal EDFs, adjusted to nuclear ground-state properties and extended to take into account correlations related to symmetry restoration and fluctuations of collective variables, describes not only general features of shape transitions but also the unique behavior of excitation spectra and transition rates at the critical point of quantum shape phase transition. In particular, the particle-number projected GCM spectra, intraband and interband $B(E2)$ values for ^{148,150,152}Nd were found in excellent agreement with data and close to the X(5)-model predictions for ^{150}Nd. The self-consistent GCM calculation based on the relativistic density functional PC-F1 [24] predicted the shape phase transition precisely at the isotope ^{150}Nd, in agreement with empirical evidence for the realization of X(5) in the $N = 90$ rare-earth isotones [5,6].

X(5) denotes a particular model for a first-order QPT between spherical and axially deformed shapes, based on the assumption of a separable potential $V(\beta, \gamma) = V_\beta(\beta) + V_\gamma(\gamma)$. By neglecting the small barrier between the competing spherical and deformed minima, i.e., taking an infinite square well in the variable β, and assuming an axially stabilized potential $V_\gamma(\gamma)$, an approximate analytic solution is obtained at the point of phase transition [14]. The microscopic axially symmetric potential for ^{150}Nd, calculated with self-consistent mean-field models (cf. Fig. 1 in Ref. [22]) is, of course, more realistic than the infinite square well considered by Iachello in Ref. [14]. First, although it displays a wide flat minimum in β on the prolate side, the flat bottom of the potential does not start at $\beta = 0$, i.e., the coexisting shapes do not include the spherical configuration. In this respect the microscopic potential is closer to the generalization of the axially symmetric X(5) solution for the collective Bohr Hamiltonian to the transition path between X(5) and the rigid-rotor limit, represented by infinite square-well potentials over a confined range of values $\beta_M > \beta_m \geqslant 0$ (confined β-soft potential, β_m and β_M denote the positions of the inner and outer walls on the β axis, respectively) [25]. Second, the microscopic potential well has softer walls compared to the X(5) square well. The unrealistic features introduced by the hard wall of the square well were analyzed in Ref. [26], and it was noted that the compression of the wave function against the well wall induces effects in spectra approximating rigid β deformation.

More importantly, the GCM calculation of Ref. [22] was restricted to axially symmetric shapes ($\gamma = 0$). We note that an exactly separable γ-rigid version (with $\gamma = 0$) of the X(5) model has been constructed in Ref. [27]. Although the original X(5) solution relied on an approximate separation of the potential in the variables β and γ [14], the exact diagonalization of the Bohr Hamiltonian with a β-soft, axially stabilized potential, carried out in Ref. [26], has shown that many properties of the solution are dominated by β-γ coupling induced by the kinetic energy operator. Band-head excitation energies, energy spacings within the bands, and transition strengths are strongly dependent on the γ stiffness of the potential. The importance of the explicit treatment of the triaxial degree of freedom, i.e., inclusion of β-γ coupling, was also emphasized in two recent studies [20,21] that used the self-consistent Hartree-Fock-Bogoliubov model, based on the finite-range and density-dependent Gogny interaction, to generate potential energy surfaces in the β-γ plane. In addition, in Ref. [20] excitation spectra of Nd isotopes were calculated using the GCM with particle-number and angular-momentum projected axially symmetric wave functions. However, although GCM configuration mixing of axially symmetric mean-field states is routinely performed in studies of collective excitation spectra, the application of this method to triaxial shapes is a much more difficult problem. Only very recently has a model been introduced [28], based on triaxial mean-field states, projected on particle number and angular momentum, and mixed by the generator coordinate method.

The numerical implementation of the model is rather complex, and applications to medium-heavy and heavy nuclei are still computationally too demanding. An alternative approach is the explicit solution of the collective Hamiltonian in five dimensions, with deformation-dependent parameters determined from microscopic self-consistent mean-field calculations. This approach will be used in the present study.

In this work we therefore extend the analysis of shape transitions in Nd isotopes of Ref. [22], to the region $Z = 60, 62, 64$ with $N \approx 90$ and include the explicit treatment of both β and γ degrees of freedom. Collective excitation spectra and transition probabilities are calculated starting from a five-dimensional collective Hamiltonian for quadrupole vibrational and rotational degrees of freedom, with parameters determined by constrained self-consistent relativistic mean-field calculations for triaxial shapes.

An outline of the theoretical framework is included in Sec. II: the method of solution of the eigenvalue problem of the general collective Hamiltonian, and the calculation of the mass parameters, moments of inertia, and zero-point energy corrections. In Sec. III we present a detailed study of shape transitions in the $N \approx 90$ rare-earth nuclei. Theoretical results are compared with experimental excitation spectra and transition rates, as well as with the X(5) approximate solution at the point of first-order quantum phase transition. Section IV presents a summary and an outlook for future studies.

II. COLLECTIVE HAMILTONIAN IN FIVE DIMENSIONS

In Ref. [29] we have developed a model for the solution of the eigenvalue problem of a five-dimensional collective Hamiltonian for quadrupole vibrational and rotational degrees of freedom, with parameters determined by constrained self-consistent relativistic mean-field calculations for triaxial shapes. The five quadrupole collective coordinates are parameterized in terms of two deformation parameters β and γ, and three Euler angles $(\phi,\ \theta,\ \psi) \equiv \Omega$, which define the orientation of the intrinsic principal axes in the laboratory frame. The collective Hamiltonian can be written in the form:

$$\hat{H} = \hat{T}_{\rm vib} + \hat{T}_{\rm rot} + V_{\rm coll}, \tag{1}$$

with the vibrational kinetic energy:

$$\begin{aligned}\hat{T}_{\rm vib} = -\frac{\hbar^2}{2\sqrt{wr}}\Bigg\{ &\frac{1}{\beta^4}\Bigg[\frac{\partial}{\partial\beta}\sqrt{\frac{r}{w}}\beta^4 B_{\gamma\gamma}\frac{\partial}{\partial\beta} \\ &-\frac{\partial}{\partial\beta}\sqrt{\frac{r}{w}}\beta^3 B_{\beta\gamma}\frac{\partial}{\partial\gamma}\Bigg] \\ &+\frac{1}{\beta\sin 3\gamma}\Bigg[-\frac{\partial}{\partial\gamma}\sqrt{\frac{r}{w}}\sin 3\gamma\, B_{\beta\gamma}\frac{\partial}{\partial\beta} \\ &+\frac{1}{\beta}\frac{\partial}{\partial\gamma}\sqrt{\frac{r}{w}}\sin 3\gamma\, B_{\beta\beta}\frac{\partial}{\partial\gamma}\Bigg]\Bigg\},\end{aligned} \tag{2}$$

and rotational kinetic energy:

$$\hat{T}_{\rm rot} = \frac{1}{2}\sum_{k=1}^{3}\frac{\hat{J}_k^2}{\mathcal{I}_k}. \tag{3}$$

$V_{\rm coll}$ is the collective potential. $\hat{J}_k$ denotes the components of the angular momentum in the body-fixed frame of a nucleus, and the mass parameters $B_{\beta\beta}$, $B_{\beta\gamma}$, $B_{\gamma\gamma}$, as well as the moments of inertia $\mathcal{I}_k$, depend on the quadrupole deformation variables β and γ:

$$\mathcal{I}_k = 4B_k\beta^2\sin^2(\gamma - 2k\pi/3). \tag{4}$$

Two additional quantities that appear in the expression for the vibrational energy: $r = B_1B_2B_3$ and $w = B_{\beta\beta}B_{\gamma\gamma} - B_{\beta\gamma}^2$, determine the volume element in the collective space. The Hamiltonian Eq. (1) describes quadrupole vibrations, rotations, and the coupling of these collective modes. The corresponding eigenvalue problem is solved using an expansion of eigenfunctions in terms of a complete set of basis functions that depend on the deformation variables β and γ, and the Euler angles ϕ, θ and ψ [30].

The dynamics of the collective Hamiltonian is governed by the seven functions of the intrinsic deformations β and γ: the collective potential, the three mass parameters $B_{\beta\beta}$, $B_{\beta\gamma}$, $B_{\gamma\gamma}$, and the three moments of inertia $\mathcal{I}_k$. These functions are determined by the choice of a particular microscopic nuclear energy-density functional or effective interaction. As in our previous study of axial shape transitions in Nd isotopes [22], also in this work we use the relativistic functional PC-F1 (point-coupling Lagrangian) [24] in the particle-hole channel, and a density-independent δ force is the effective interaction in the particle-particle channel. The parameters of the PC-F1 functional and the pairing strength constants V_n and V_p have been adjusted simultaneously to ground-state observables (binding energies, charge and diffraction radii, surface thickness, and pairing gaps) of spherical nuclei [24], with pairing correlations treated in the BCS approximation.

The map of the energy surface as function of the quadrupole deformation is obtained by imposing constraints on the axial and triaxial mass quadrupole moments. The method of quadratic constraints uses an unrestricted variation of the function

$$\langle H\rangle + \sum_{\mu=0,2} C_{2\mu}\left(\langle\hat{Q}_{2\mu}\rangle - q_{2\mu}\right)^2, \tag{5}$$

where $\langle H\rangle$ is the total energy and $\langle\hat{Q}_{2\mu}\rangle$ denotes the expectation value of the mass quadrupole operator:

$$\hat{Q}_{20} = 2z^2 - x^2 - y^2 \quad \text{and} \quad \hat{Q}_{22} = x^2 - y^2. \tag{6}$$

$q_{2\mu}$ is the constrained value of the multipole moment and $C_{2\mu}$ the corresponding stiffness constant [23].

The moments of inertia are calculated according to the Inglis-Belyaev formula: [31,32]

$$\mathcal{I}_k = \sum_{i,j}\frac{(u_iv_j - v_iu_j)^2}{E_i + E_j}\langle i|\hat{J}_k|j\rangle|^2 \quad k = 1, 2, 3, \tag{7}$$

where k denotes the axis of rotation and the summation runs over the proton and neutron quasiparticle states. The quasiparticle energies E_i, occupation probabilities v_i, and single-nucleon wave functions ψ_i are determined by solutions of the constrained relativistic mean-field (RMF) plus BCS equations. The mass parameters associated with the two quadrupole collective coordinates $q_0 = \langle\hat{Q}_{20}\rangle$ and $q_2 = \langle\hat{Q}_{22}\rangle$

are also calculated in the cranking approximation [33]

$$B_{\mu\nu}(q_0, q_2) = \frac{\hbar^2}{2}\left[\mathcal{M}_{(1)}^{-1}\mathcal{M}_{(3)}\mathcal{M}_{(1)}^{-1}\right]_{\mu\nu}, \tag{8}$$

with

$$\mathcal{M}_{(n),\mu\nu}(q_0, q_2) = \sum_{i,j}\frac{\langle i|\hat{Q}_{2\mu}|j\rangle\langle j|\hat{Q}_{2\nu}|i\rangle}{(E_i + E_j)^n}(u_i v_j + v_i u_j)^2. \tag{9}$$

The collective energy surface includes the energy of zero-point motion (ZPE) that corresponds to a superposition of zero-point motion of individual nucleons in the single-nucleon potential. The ZPE correction depends on the deformation and includes terms originating from the vibrational and rotational kinetic energy and a contribution of potential energy

$$\Delta V(q_0, q_2) = \Delta V_{\rm vib}(q_0, q_2) + \Delta V_{\rm rot}(q_0, q_2) + \Delta V_{\rm pot}(q_0, q_2). \tag{10}$$

The latter is much smaller than the kinetic energy contribution and is usually neglected. The vibrational and rotational ZPE are calculated in the cranking approximation [33], i.e., on the same level of approximation as the mass parameters and the moments of inertia. The potential $V_{\rm coll}$ in the collective Hamiltonian Eq. (1) is obtained by subtracting the ZPE corrections from the total energy that corresponds to the solution of constrained RMF+BCS equations [cf. Eq. (5)], at each point on the triaxial deformation plane:

$$V_{\rm coll}(q_0, q_2) = E_{\rm tot}(q_0, q_2) - \Delta V_{\rm vib}(q_0, q_2) - \Delta V_{\rm rot}(q_0, q_2). \tag{11}$$

III. SHAPE PHASE TRANSITIONS IN THE $N \approx 90$ REGION

The present study considers the Nd, Sm, and Gd nuclei with $N \approx 90$. These isotopic chains display transitions from spherical to deformed shapes, and experimental evidence has recently been reported [15,34,35] for the $N = 90$ isotones: ^{150}Nd, ^{152}Sm, ^{154}Gd lying close to the point of first-order QPT. We will first extend our analysis of Ref. [22] of the Nd isotopic chain to explicitly include the triaxial degree of freedom. The microscopic picture of shape phase transitions at $N = 90$ will be analyzed in detail for the Nd nuclei, and in the remainder of this section the most interesting results for the Sm and Gd isotopic chains will be presented.

In Fig. 1 we display the self-consistent RMF+BCS triaxial quadrupole binding energy maps of the even-even $^{144-154}$Nd in the β-γ plane ($0 \leqslant \gamma \leqslant 60^\circ$), obtained by imposing constraints on expectation values of the quadrupole moments $\langle\hat{Q}_{20}\rangle$ and $\langle\hat{Q}_{22}\rangle$ [cf. Eq. (5)]. Filled circle symbols denote absolute minima; all energies are normalized with respect to the binding energy of the absolute minimum. The contours join points on the surface with the same energy. The energy maps nicely illustrate the gradual increase of deformation of the prolate minimum with increasing number of neutrons, from the spherical ^{144}Nd to the strongly deformed ^{154}Nd, and the evolution of the γ dependence of the potentials. With increasing neutron number the Nd isotopes remain prolate deformed in the lowest state, i.e., the shape evolution corresponds, in the language of the interacting boson model, to a transition between the U(5) and SU(3) limits of the Casten symmetry triangle [5,6]. One notes, however, the appearance of oblate minima in ^{152}Nd and ^{154}Nd. An important feature of the energy maps shown in Fig. 1 is the extended flat minimum around $\beta \approx 0.3$ in ^{150}Nd. This is seen even more clearly in the axial maps of Fig. 2, where we plot the binding energies as functions of the axial deformation parameter β. Energies are normalized with respect to the binding energy of the absolute minimum for a given isotope. Negative values of β correspond to the oblate ($\beta > 0$, $\gamma = 60^\circ$) axis on the β-γ plane. The prolate minimum gradually shifts to larger deformation and saturates at $\beta \approx 0.35$ in ^{152}Nd and ^{154}Nd. It is interesting that for these two nuclei the calculation also predicts the same deformation $\beta \approx -0.3$ of the oblate minima. The difference is in the barriers separating the prolate and oblate minima: 6 MeV for ^{152}Nd and more than 7 MeV for ^{154}Nd. For ^{150}Nd, however, the flat prolate minimum extends in the interval $0.2 \leqslant \beta \leqslant 0.4$, whereas the oblate minimum at $\beta \approx -0.2$ is not a true minimum but rather a saddle point in the β-γ plane (cf. Fig. 1). This is illustrated in Fig. 3, where we plot the binding energy curves of ^{150}Nd as functions of the deformation parameter γ, for two values of the axial deformation $\beta = 0.2$ and 0.25. In the region of the flat prolate minimum the potential displays a parabolic dependence on γ for $\gamma \leqslant 30^\circ$ but flattens with increasing γ because, of course, it must be periodic with a period $2\pi/3$. The difference between the two curves plotted in Fig. 3 shows that the γ potential is not completely independent of β, as it was originally assumed for the X(5) model in Ref. [14]. We note that both in the test of the X(5) for the γ degree of freedom of Ref. [40], as well as in the study of the validity of the approximate separation of variables introduced with the X(5) model [26], the potential in γ was chosen to be a harmonic oscillator potential.

Potential energy surfaces similar to those shown in Fig. 1 were also obtained in two recent studies [20,21] that used the self-consistent Hartree-Fock-Bogoliubov (HFB) model, based on the finite-range and density-dependent Gogny interaction. However, compared to the results shown in Figs. 1 and 2, the flat prolate minimum in ^{150}Nd is less pronounced in the HFB calculation with the Gogny force. By performing the corresponding GCM calculation with particle-number and angular-momentum projected axially symmetric wave functions, the authors of Ref. [20] show that, rather than ^{150}Nd, the excitation energies and transition probabilities for ^{148}Nd are actually closer to the X(5) model predictions. In fact, they notice that intrinsic potentials that differ from the one considered in the original X(5) model [14] (wide flat minimum in β starting at $\beta = 0$) lead to excitation spectra and transition rates similar to the X(5) predictions and thus question the use of the axial deformation β as order parameter of a shape phase transition.

Starting from constrained self-consistent solutions, i.e., using single-particle wave functions, occupation probabilities, and quasiparticle energies that correspond to each point on the energy surfaces shown in Fig. 1, the parameters that determine the collective Hamiltonian (mass parameters $B_{\beta\beta}$, $B_{\beta\gamma}$, $B_{\gamma\gamma}$, three moments of inertia $\mathcal{I}_k$, as well as the zero-point energy

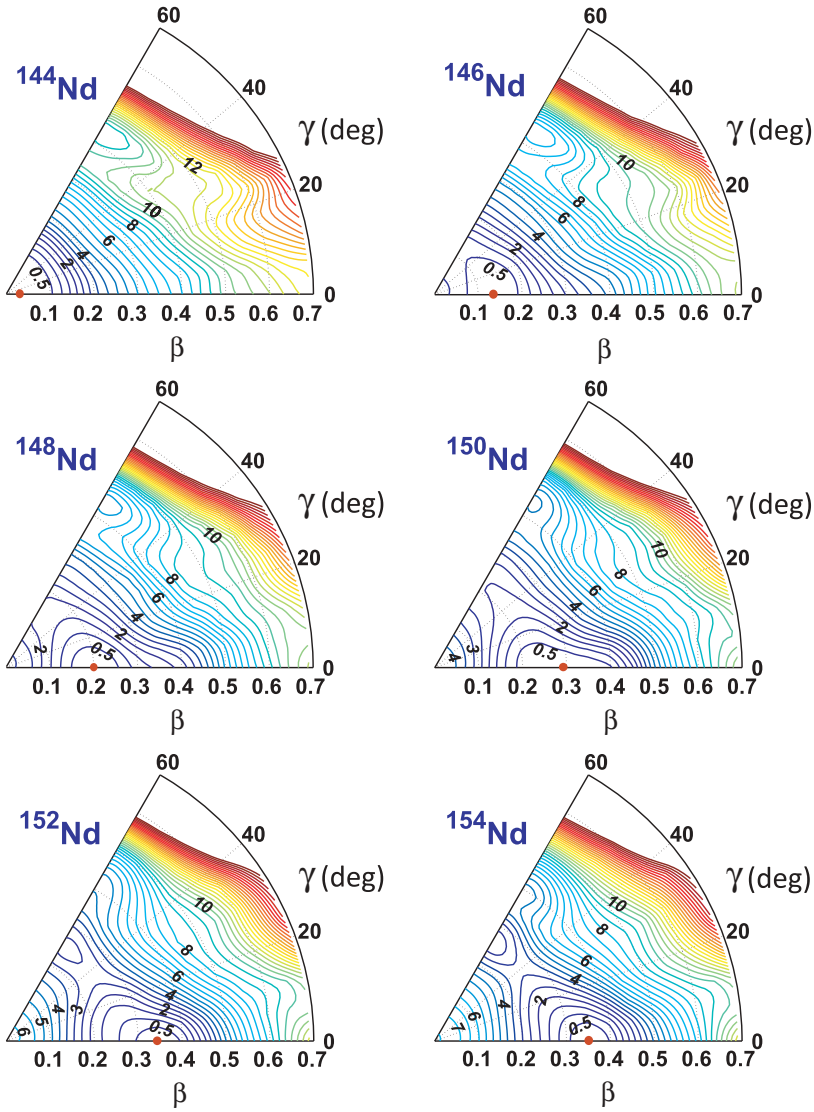

FIG. 1. (Color online) Self-consistent RMF+BCS triaxial quadrupole binding energy maps of the even-even $^{144-154}$Nd isotopes in the β-γ plane ($0 \leqslant \gamma \leqslant 60^{\circ}$). All energies are normalized with respect to the binding energy of the absolute minimum (red filled circle). The contours join points on the surface with the same energy (in MeV).

corrections) are calculated as functions of the deformations β and γ. The diagonalization of the resulting Hamiltonian yields the excitation energies E^I_α and the collective wave functions:

$$\Psi^{IM}_\alpha(\beta,\gamma,\Omega) = \sum_{K\in\Delta I} \psi^I_{\alpha K}(\beta,\gamma)\Phi^I_{MK}(\Omega). \tag{12}$$

The angular part corresponds to linear combinations of the Wigner functions

$$\Phi^I_{MK}(\Omega)=\sqrt{\frac{2I+1}{16\pi^2(1+\delta_{K0})}}\left[D^{I*}_{MK}(\Omega)+(-1)^I D^{I*}_{M-K}(\Omega)\right], \tag{13}$$

and the summation in Eq. (12) is over the allowed set of the K values:

$$\Delta I = \begin{cases} 0,2,\ldots,I & \text{for} \quad I \bmod 2 = 0 \\ 2,4,\ldots,I-1 & \text{for} \quad I \bmod 2 = 1 \end{cases}. \tag{14}$$

In addition to the yrast ground-state band, in deformed and transitional nuclei excited states are usually also assigned to (quasi-) β and γ bands. This is done according to the distribution of the angular-momentum projection K quantum number. Excited states with predominant $K = 2$ components in the wave function are assigned to the γ band, whereas the β band comprises states above the yrast characterized by dominant $K = 0$ components. The mixing of different intrinsic configurations in the state $|\alpha I\rangle$ can be determined from the distribution of the projection K of the angular momentum I on the z axis in the body-fixed frame:

$$N_K = 6\int_0^{\pi/3}\int_0^{\infty} \left|\psi^I_{\alpha,K}(\beta,\gamma)\right|^2 \beta^4 |\sin 3\gamma| d\beta d\gamma, \tag{15}$$

where the components $\psi^I_{\alpha,K}(\beta,\gamma)$ are defined in Eq. (12). When K is a good quantum number, only one of the integrals Eq. (15) will give a value close to 1. A broader distribution of N_K values in the state $|\alpha I\rangle$ provides a measure of mixing of intrinsic configurations.

Before comparing the calculated excitation spectrum of ^{150}Nd with data and X(5) model predictions, we will consider some characteristic signatures of shape transitions in Nd isotopes. One of the distinct features of shape transitions is the ratio between the excitation energies of the first 4^+ and

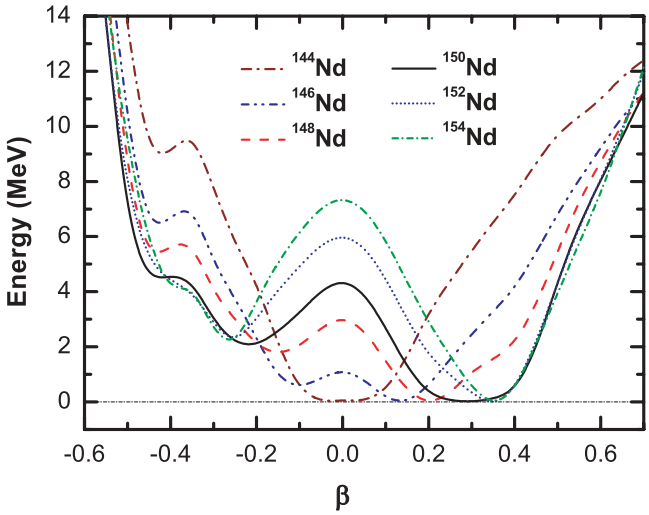

FIG. 2. (Color online) Self-consistent RMF+BCS binding energy curves of the even-even $^{144-154}$Nd isotopes as functions of the axial deformation parameter β. Energies are normalized with respect to the binding energy of the absolute minimum for a given isotope. Negative values of β correspond to the oblate ($\beta > 0,\ \gamma = 60°$) axis on the β-γ plane.

2^+ states along an isotopic chain. For a transition between spherical and axially deformed shapes, this quantity varies from the value $R_{4/2} \equiv E(4_1^+)/E(2_1^+) = 2$ characteristic for a spherical vibrator [U(5) symmetry limit], to $R_{4/2} = 3.33$ for a well-deformed axial rotor [SU(3) symmetry limit]. In the left panel of Fig. 4 we plot the theoretical values of $R_{4/2}$ for the six Nd isotopes, calculated from the spectrum of the collective Hamiltonian with mass parameters, moments of inertia, and potentials determined by the PC-F1 density functional, in comparison with experimental values. The calculation reproduces in detail the rapid increase of $R_{4/2}$ from the spherical value of ≈1.9 in ^{144}Nd to ≈3.3 characteristic for the well-deformed rotors ^{152}Nd and ^{154}Nd. For the $N = 90$ isotope, in particular,

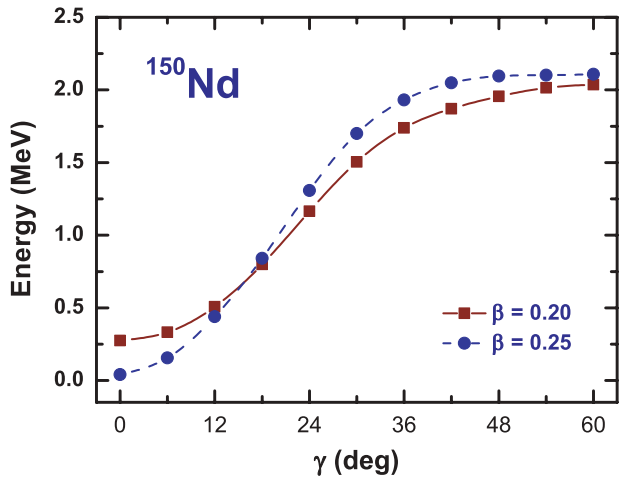

FIG. 3. (Color online) Self-consistent RMF+BCS binding energy curves of the ^{150}Nd nucleus, as functions of the deformation parameter γ for two values of the axial deformation $\beta = 0.2$ and 0.25.

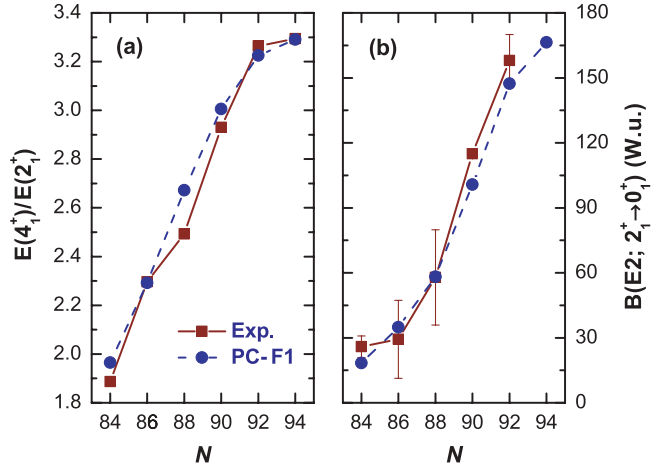

FIG. 4. (Color online) Evolution of the characteristic collective observables $R_{4/2}$ and $B(E2; 2_1^+ \rightarrow 0_1^+)$ (in W.u.) with neutron number in Nd isotopes. The microscopic values calculated with the PC-F1 energy-density functional are shown in comparison with data [34,41, 42].

the calculated $R_{4/2} = 3$ and experimental $R_{4/2} = 2.93$ values, are very close to the characteristic, parameter-free, X(5) model prediction $R_{4/2} = 2.91$ [14]. Note, however, that our microscopic results for $R_{4/2}$, as well as other characteristic quantities, include the effect of β-γ coupling, absent in the original X(5)-symmetry model. The panel on the right of Fig. 4 illustrates the evolution of another characteristic collective observable with neutron number: $B(E2; 2_1^+ \rightarrow 0_1^+)$ (in W.u.). The important result here is not only that the calculation reproduces the swift increase of the empirical $B(E2)$ values from less than 30 W.u. in ^{144}Nd, to more than 160 W.u. in ^{152}Nd but also that the calculation is completely parameter free. Namely an important advantage of using structure models based on self-consistent mean-field single-particle solutions is the fact that physical observables, such as transition probabilities and spectroscopic quadrupole moments, are calculated in the full configuration space and there is no need for effective charges. Using the bare value of the proton charge in the electric quadrupole operator $\hat{\mathcal{M}}(E2)$, the transition probabilities between eigenstates of the collective Hamiltonian can be directly compared with data. This is in contrast to, for instance, algebraic (interacting boson model) or shell-model approaches, that explicitly consider only valence nucleons and, therefore, calculate transition rates by adjusting the effective charges to reproduce some empirical values. For example, the X(5) predictions for transition strengths are normalized to the experimental $B(E2; 2_1^+ \rightarrow 0_1^+)$. We also note that the present results, both for $R_{4/2}$ and $B(E2; 2_1^+ \rightarrow 0_1^+)$, are in better agreement with data than those obtained in the axial GCM calculation with the Gogny force in Ref. [20]. In particular, the transition from spherical to well-deformed Nd nuclei is less abrupt than in the axial GCM calculation and, therefore, the solutions of the collective Hamiltonian in five dimensions including β-γ coupling, describe much better the transitional nuclei ^{148}Nd and ^{150}Nd.

In Fig. 5 we display the isotopic dependence of the first excited 0^+ state, and the ratio $E(6_1^+)/E(0_2^+)$ in Nd nuclei.

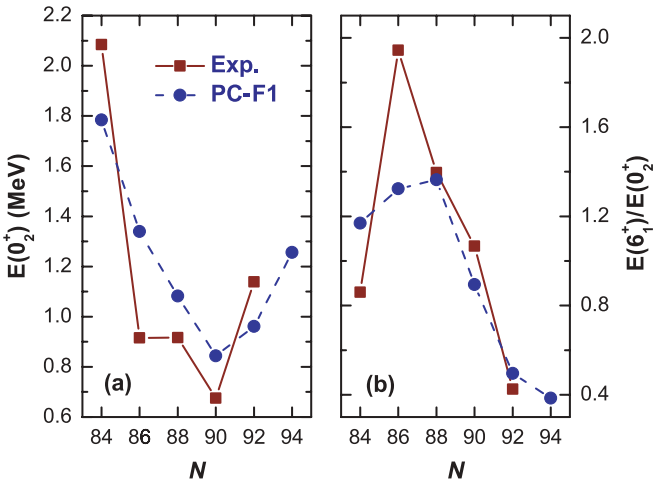

FIG. 5. (Color online) Evolution of the first excited 0^+ state and the ratio $E(6_1^+)/E(0_2^+)$ with neutron number in Nd isotopes. The microscopic values calculated with the PC-F1 energy-density functional are compared to data [41,42].

The microscopic excitation energies calculated with the PC-F1 energy-density functional are compared with experimental values. The calculation reproduces the empirical trend and, in particular, it predicts that the first excited 0^+ state has the lowest excitation energy at $N = 90$, in agreement with data. With the exception of the very low 0_2^+ state in ^{146}Nd, the calculated excitation energies are also in quantitative agreement with experimental values. The fact that the bandhead 0_2^+ of the quasi-β band has the lowest excitation energy in ^{150}Nd can be attributed to the softness (flatness) of the potential with respect to β deformation (cf. Figs. 1 and 2). With the increase of the stiffness of the potential in ^{152}Nd and ^{154}Nd, the position of the β band is shifted to higher excitation energies, and the ratio $E(6_1^+)/E(0_2^+)$ decreases to less than 1/2.

The prediction of a near degeneracy of the 6_1^+ level of the ground-state band and the first excited 0^+ state is another key signature of the X(5) model [5,6]. In a very recent study of empirical order parameters for first-order nuclear QPT [36], Bonatsos *et al.* have shown that the ratio $E(6_1^+)/E(0_2^+)$ presents an effective order parameter of a first-order phase transition and takes the special value of $\approx$1 close to the phase transition point. Furthermore, results of extensive IBM calculations with large boson number N_B show that the degeneracy of $E(0_2^+)$ and $E(6_1^+)$ is a signature of a *line* of first-order transitions that extends across the Casten symmetry triangle. The ratios $E(6_1^+)/E(0_2^+)$ obtained with the PC-F1 energy-density functional are compared to the experimental values in Fig. 5(b). We note that the calculation reproduces the abrupt decrease of this quantity between ^{148}Nd and ^{152}Nd, with a value close to 1 in ^{150}Nd. The isotopic dependence of the theoretical values corresponds to the one predicted for a first-order phase transition in Ref. [36].

In Fig. 6 we compare the spectrum of the collective Hamiltonian for ^{150}Nd with available data for positive-parity states [34,41,42] and with the predictions of the X(5) model. For the moments of inertia of the collective Hamiltonian we have multiplied the Inglis-Belyaev values Eq. (7) with a common factor determined in such a way that the calculated energy of the 2_1^+ state coincides with the experimental value. In deformed nuclei, to a good approximation, the enhancement of the effective moment of inertia scales the relative excitation energies within each band by a common factor but otherwise leaves the bandhead of the β band (0_2^+) unaltered. Of course, this simple relation between the scaling of effective moments of inertia and excitation energies within each band would be exact only if rotational and vibrational degrees of freedom were decoupled. The degree of mixing between bands can be inferred from the distribution of K components (projection of the angular momentum on the body fixed-symmetry axis) of collective wave functions (cf. Table I). The transition rates are calculated in the full configuration space using bare charges. The inclusion of an additional scale parameter in our calculation was necessary because of the well-known fact that the Inglis-Belyaev (IB) formula (7) predicts effective

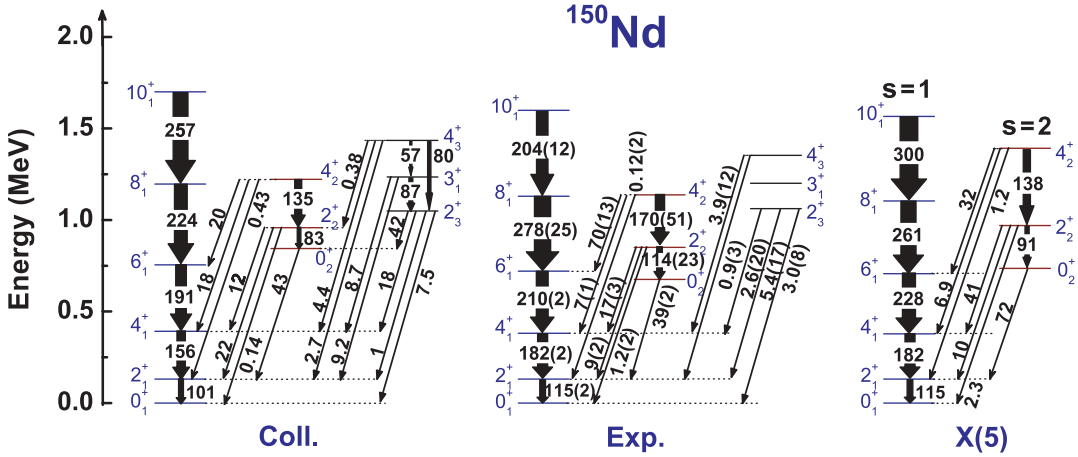

FIG. 6. (Color online) The spectrum of ^{150}Nd calculated with the PC-F1 relativistic density functional (left) compared with the data [34] (middle) and the X(5)-symmetry predictions (right) for the excitation energies and intraband and interband $B(E2)$ values (in W.u.) of the ground-state ($s = 1$) and β_1 ($s = 2$) bands. The theoretical spectra are normalized to the experimental energy of the state 2_1^+, and the X(5) transition strengths are normalized to the experimental $B(E2; 2_1^+ \rightarrow 0_1^+)$.

TABLE I. Distribution of the K-components $K = 0, 2, 4$ (projection of the angular momentum on the body fixed-symmetry axis) in percentage (%), for the collective wave functions of the lowest three bands in ^{150}Nd, ^{152}Sm, and ^{154}Gd.

	^{150}Nd			^{152}Sm			^{154}Gd		
	$K=0$	$K=2$	$K=4$	$K=0$	$K=2$	$K=4$	$K=0$	$K=2$	$K=4$
2_1^+	99.8	0.2	0	99.9	0.1	0	99.9	0.1	0
4_1^+	99.2	0.8	0	99.7	0.3	0	99.6	0.4	0
6_1^+	98.5	1.5	0	99.3	0.7	0	98.9	1.1	0
8_1^+	98.0	1.9	0.1	98.9	1.1	0	98.1	1.9	0
10_1^+	98.0	1.9	0.1	98.4	1.6	0	97.0	3.0	0
2_2^+	53.5	46.5	0	91.1	8.9	0	96.1	3.9	0
4_2^+	77.4	21.0	1.6	85.5	13.9	0.6	92.7	7.1	0.2
6_2^+	79.7	18.2	1.7	80.1	19.0	0.9	89.9	9.7	0.4
2_3^+	47.7	52.3	0	9.5	90.5	0	4.2	95.8	0
3_1^+	0	100	0	0	100	0	0	100	0
4_3^+	26.4	68.2	5.4	15.5	83.0	1.5	8.1	91.0	0.9
5_1^+	0	95.5	4.5	0	98.8	1.2	0	99.0	1.0
6_3^+	27.2	61.8	8.8	21.0	77.1	1.7	11.2	87.0	1.7

moments of inertia that are considerably smaller than empirical values. More realistic values are only obtained if one uses the Thouless-Valatin (TV) formula, but this procedure is computationally much more demanding, and it has not been implemented in the current version of the model. Here we rather follow the prescription of Ref. [37] where, by comparing the TV and IB moments of inertia as functions of the axial deformation for superdeformed bands in the $A = 190$–198 mass region, it was shown that the Thouless-Valatin correction to the perturbative expression IB is almost independent of deformation and does not include significant new structures in the moments of inertia. It was thus suggested that the moments of inertia to be used in the collective Hamiltonian can be simply related to the IB values through the minimal prescription: $\mathcal{I}_k(q) = \mathcal{I}_k^{IB}(q)(1+\alpha)$, where q denotes the generic deformation parameter and α is a constant that can be determined in a comparison with data. The value $\alpha \approx 0.4$ used for the excitation spectrum of ^{150}Nd is comparable to those determined in the mass $A = 190 - 198$ region [37].

When the IB effective moment of inertia is renormalized to the empirical value, the excitation spectrum of the collective Hamiltonian determined by the PC-F1 density functional is in very good agreement with the available data for the ground-state band and (quasi-) β and γ bands. This is also true for the corresponding intraband and interband $B(E2)$ values except, perhaps, for the strong transition $2_3^+ \to 0_2^+$ ($\approx$42 W.u.), not seen in the experiment. Such a strong transition is probably due to the mixing between the theoretical (quasi-) β and γ bands. Table I includes the distributions of K components (projection of the angular momentum on the body fixed-symmetry axis), for the collective wave functions of the lowest three bands in ^{150}Nd, ^{152}Sm, and ^{154}Gd. For ^{150}Nd, in particular, we notice a pronounced mixing of the states 2_2^+ and 2_3^+, assigned to the β and γ bands, respectively. For higher angular momenta the mixing between the two bands is less pronounced. In addition to the results for intraband transitions, we notice the very good agreement between the theoretical and experimental value $B(E2; 0_2^+ \to 2_1^+)$. Again, we emphasize that the calculation of transition probabilities is parameter-free. Figure 6 also includes the X(5) model predictions for ground-state ($s = 1$) and $\beta_1(s = 2)$ bands of ^{150}Nd. The theoretical spectrum is normalized to the experimental energy of the state 2_1^+ and, in addition, the X(5) transition strengths are normalized to the experimental $B(E2; 2_1^+ \to 0_1^+)$. The simple X(5) model does not reproduce the data with the same accuracy as the solution of the collective Hamiltonian, especially the transition rates between bands. This could be due to the fact that ^{150}Nd is already slightly to the rotor side of the phase transition [38,39] or simply to the fact that the X(5) model does not include β-γ coupling effects. Of course, even though the ansatz for the X(5) model involves a separation of variables in the β and γ degrees of freedom, a full set of predictions for the quasi-γ band can be obtained [40]. However, this necessitates two additional parameters in the X(5) model that are adjusted, for instance, to the excitation energy of the quasi-γ band and the $\Delta K = 2$ transitions.

When compared with our particle-number projected axial GCM calculation of Ref. [22], where the same PC-F1 density functional was used, but configuration mixing included only prolate axially symmetric wave functions (cf. Fig. 2 of Ref. [22]), the full solution of the collective Hamiltonian in five dimensions displays reduced $B(E2)$ values both for interband and intraband transitions, and the β band is calculated at higher excitation energy. However, the inclusion of β-γ coupling effects does not spoil the good agreement with data. The comparison with the X(5) model predictions is also illustrated in Fig. 7 where, for the yrast states of ^{148}Nd, ^{150}Nd, and ^{152}Nd, we compare the $B(E2; L \to L-2)$ values and excitation energies calculated using the collective Hamiltonian based on the PC-F1 density functional, with the corresponding values

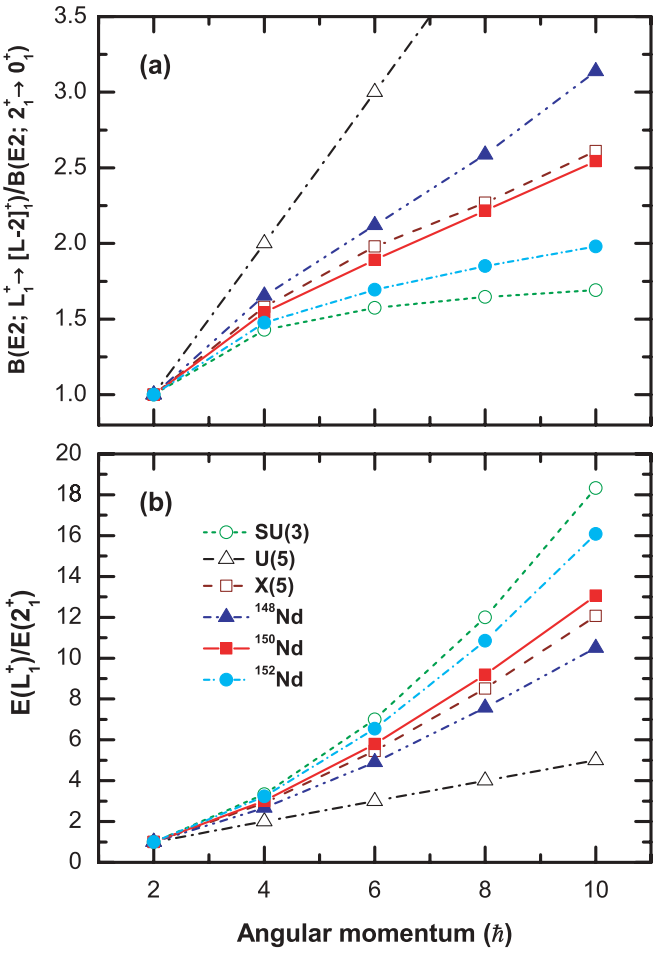

FIG. 7. (Color online) $B(E2; L \to L-2)$ values (upper panel) and excitation energies (lower panel) for the yrast states in ^{148}Nd, ^{150}Nd, and ^{152}Nd, calculated with PC-F1 and compared with those predicted by the U(5), X(5), and SU(3) symmetries (open symbols).

predicted by the U(5) and SU(3) dynamical symmetries, and the X(5) model. Obviously the $E2$ rates and excitation energies for ^{150}Nd are closest to those calculated from analytic expressions corresponding to the X(5) model. ^{148}Nd does not differ very much from the X(5) limit, whereas the yrast states of ^{152}Nd indicate that this nucleus is closer to a deformed rotor. We note, for instance, that in the case of the axial GCM model based on the Gogny interaction, the X(5) model predictions for the yrast excitation energies and transition rates were actually found to be closer to the calculated spectrum of ^{148}Nd rather than that of ^{150}Nd [20]. This comparison, of course, emphasizes the problem that the physical control parameter, i.e., the nucleon number, is not continuous and therefore in general a microscopic calculation cannot exactly reproduce the point of QPT, in contrast to phenomenological geometric or algebraic models that use continuous control parameters.

A microscopic picture of the softness of the potential with respect to β deformation and the related phenomenon of QPT in ^{150}Nd, emerges when considering the single-nucleon levels. In Figs. 8 and 9 we display the neutron single-particle levels in $^{146-152}$Nd and the neutron and proton single-particle levels in ^{150}Nd, respectively, as functions of the axial deformation parameter β. The thick dot-dashed curves denote the position of the corresponding Fermi levels. In Fig. 8 we follow the evolution of the Fermi level with the increase in neutron number. For the range of deformation $0.2 \leqslant \beta \leqslant 0.4$, in particular, the Fermi level crosses an energy interval of low level density. In ^{150}Nd both the neutron and proton Fermi levels (cf. Fig. 9) are in the region of low level density for $0.2 \leqslant \beta \leqslant 0.4$, and this result in the soft-β potential (cf. Figs. 1 and 2). With further increase of the neutron number, the corresponding Fermi level in ^{152}Nd approaches a region of high level density and the potential displays a pronounced, well-deformed minimum at $\beta \approx 0.35$. Further evidence for an abrupt change of structure between ^{150}Nd and ^{152}Nd can be clearly seen in the experimental spectra of the neighboring odd-Z nuclei: ^{151}Pm and ^{153}Pm [41]. Qualitatively very different band structures result from the coupling of the odd proton to the $N = 90$ or $N = 92$ core nuclei. In ^{153}Pm ($N = 92$) one finds regular $\Delta J = 1$ low-lying rotational bands characteristic for the limit of strong coupling. However, the lowest bands in ^{151}Pm ($N = 90$) are regular $\Delta J = 2$ sequences, and this indicates that the odd proton is coupled to a core nucleus that is soft with respect to axial deformation.

The microscopic results for the Sm and Gd isotopic chains are not very different from those of Nd nuclei, and thus in the remainder of this section we present only the most interesting features related to possible QPT. The self-consistent RMF+BCS triaxial quadrupole binding energy maps of ^{150,152,154}Sm in the β-γ plane ($0 \leqslant \gamma \leqslant 60^\circ$) are shown in Fig. 10, and those of ^{152,154,156}Gd in Fig. 11. In both cases we notice the increase of deformation of the prolate minima with increasing number of neutrons. However, in contrast to ^{150}Nd, the two $N = 90$ isotones do not display pronounced β-extended minima. This is especially the case for ^{152}Sm, whereas a more extended flat prolate minimum of the potential energy surface is calculated in ^{154}Gd. Note also that the model does not predict the occurrence of oblate minima in the $N = 92$ isotones ^{154}Sm and ^{156}Gd.

The slight change in the potentials of the two heavier $N = 90$ isotones is also reflected in the corresponding spectra of the collective Hamiltonian. Figures 12 and 13 display the spectra of ^{152}Sm and ^{154}Gd, respectively, calculated with the PC-F1 relativistic density functional, in comparison with data [15,35,41,42], and the X(5)-model predictions for the excitation energies and intraband and interband $B(E2)$ values of the ground-state ($s = 1$) and β_1 ($s = 2$) bands. For both nuclei the spectra of the collective Hamiltonian are in very good agreement with data, especially for the $E2$ transition rates. The agreement is perhaps not so good for the relative position of the β bands, which are calculated at somewhat higher excitation energies compared to data, and the effective moments of inertia of the quasi-γ bands are considerably smaller than the empirical values. As shown in Table I, the mixing between the β and γ bands is much less pronounced than in the case of ^{150}Nd. When compared to the predictions of the simple X(5) model, it is clear that the full collective Hamiltonian in five dimensions provides a more complete and accurate description of the low-energy spectra of ^{152}Sm

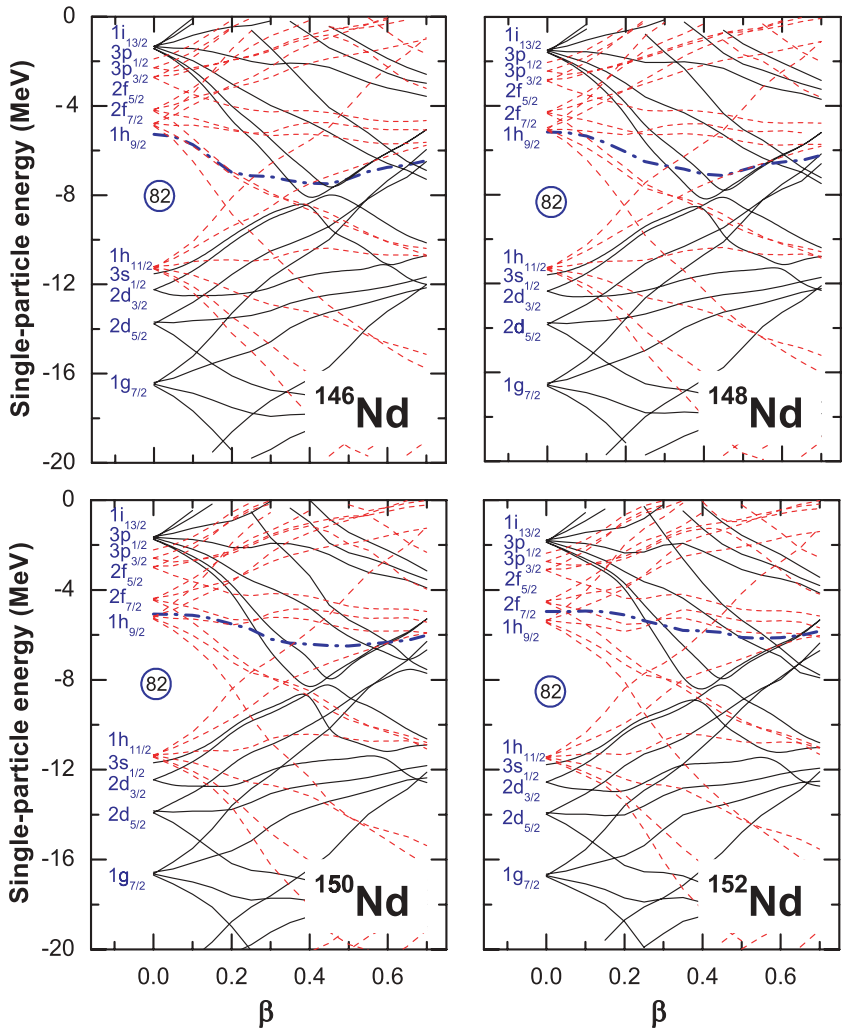

FIG. 8. (Color online) Neutron single-particle levels in Nd isotopes as functions of the axial deformation parameter β. Thick dot-dashed curves denote the position of the Fermi level.

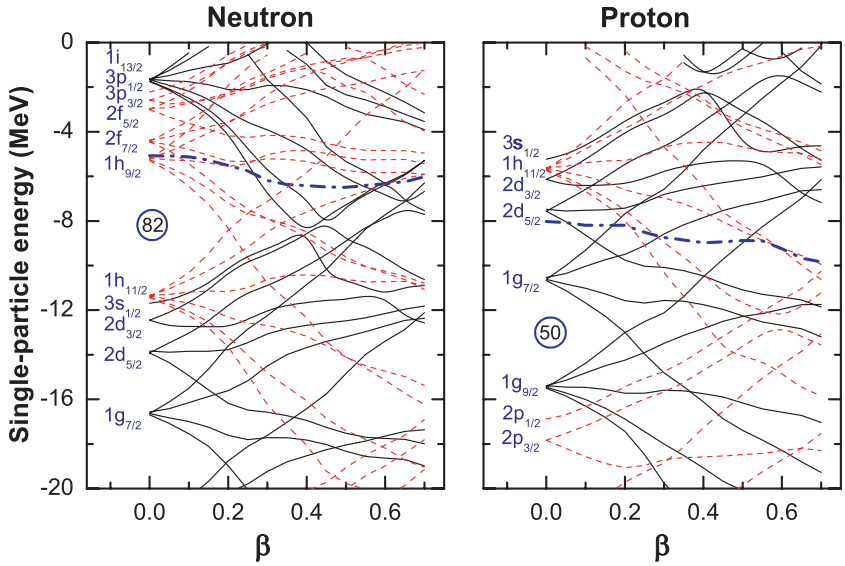

FIG. 9. (Color online) Neutron (left) and proton (right) single-particle levels in ^{150}Nd, as functions of the axial deformation parameter β. Thick dot-dashed curves denote the position of the corresponding Fermi levels.

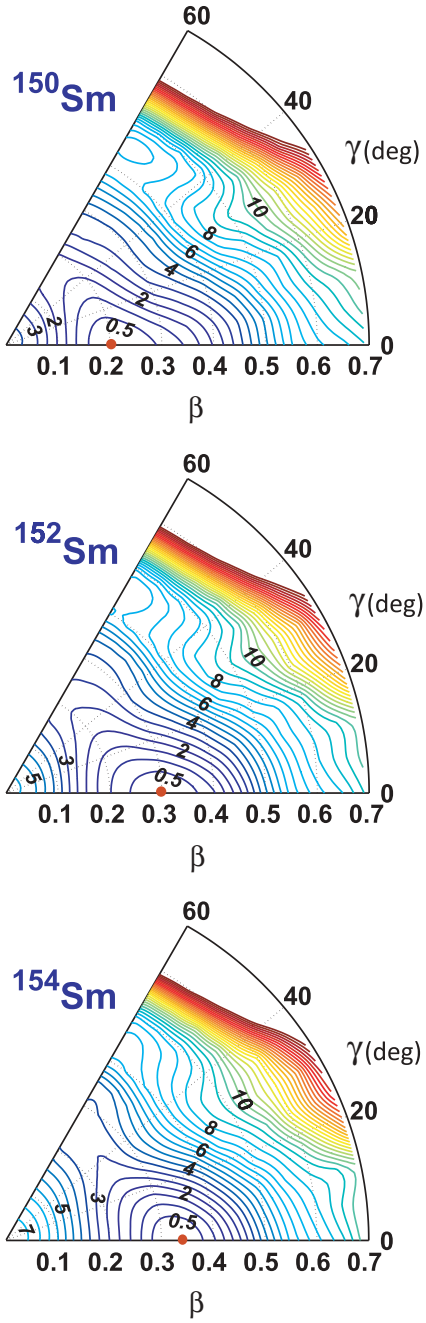

FIG. 10. (Color online) Self-consistent RMF+BCS triaxial quadrupole binding energy maps of ^{150,152,154}Sm in the β-γ plane ($0 \leqslant \gamma \leqslant 60^{\circ}$). All energies are normalized with respect to the binding energy of the absolute minimum (red filled circle). The contours join points on the surface with the same energy (in MeV).

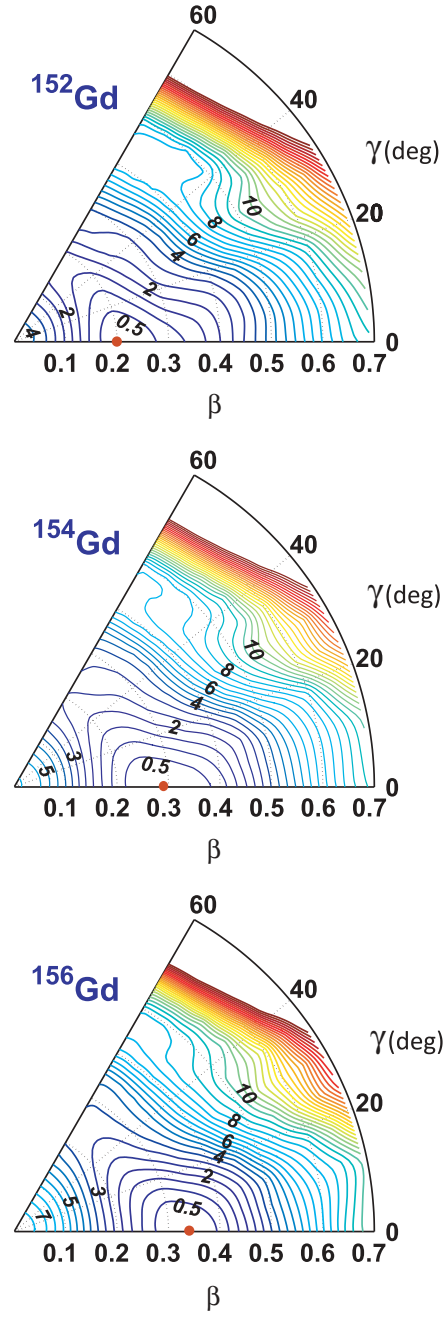

FIG. 11. (Color online) Same as described in the caption to Fig. 10 but for the isotopes ^{152,154,156}Gd.

and ^{154}Gd, especially for interband transitions between the β and ground-state bands. The comparison with X(5) is further illustrated in Figs. 14 and 15, where we plot the microscopic $B(E2; L \rightarrow L-2)$ values and excitation energies of yrast states of Sm and Gd $N \approx 90$ nuclei. Although in the case of Nd isotopes the X(5) limit was very close to the results for ^{150}Nd, for Sm and Gd the X(5) predictions lie in between the results obtained with the collective Hamiltonian for the $N = 88$ and $N = 90$ isotopes.

IV. SUMMARY AND OUTLOOK

The structural evolution of nuclei with neutron and/or proton number presents interesting shape transition phenomena, and in a number of systems signatures of first- and second-order quantum shape phase transitions have been observed. In this work we have applied the recently developed model for the solution of a five-dimensional collective Hamiltonian

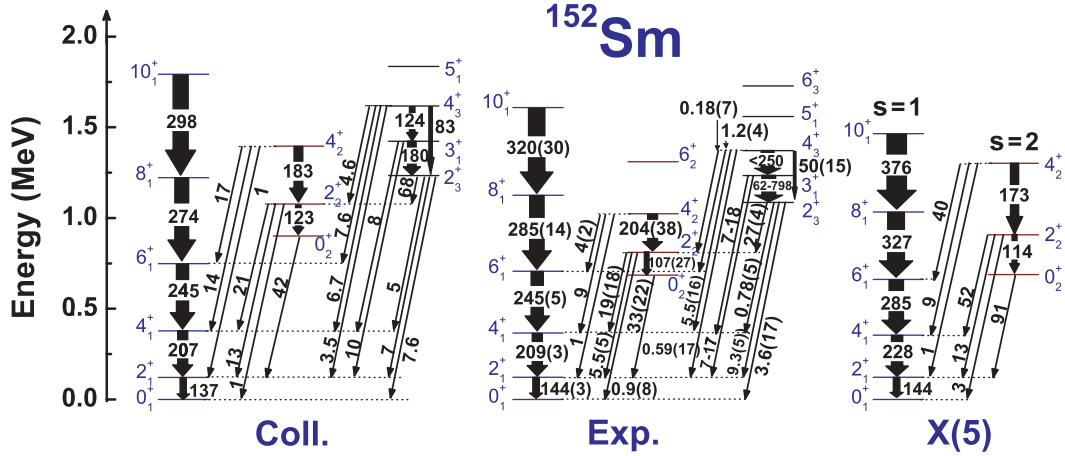

FIG. 12. (Color online) The spectrum of ^{152}Sm calculated with the PC-F1 relativistic density functional (left) compared with data (middle) and the X(5)-symmetry predictions (right) for the excitation energies and intraband and interband $B(E2)$ values (in W.u.) of the ground-state ($s = 1$) and β_1 ($s = 2$) bands. The theoretical spectra are normalized to the experimental energy of the state 2_1^+, and the X(5) transition strengths are normalized to the experimental $B(E2; 2_1^+ \rightarrow 0_1^+)$.

for quadrupole vibrational and rotational degrees of freedom, with parameters determined by constrained self-consistent relativistic mean-field calculations for triaxial shapes, to a microscopic study of shape transitions in Nd, Sm, and Gd isotopes with neutron number $N \approx 90$. Available data on excitation spectra and transition rates indicate that the $N = 90$ isotones (^{150}Nd, ^{152}Sm, and ^{154}Gd) are located close to the point of first-order QPT between spherical to axially deformed shapes.

Starting from self-consistent triaxial quadrupole binding energy maps in the β-γ plane, calculated with the PC-F1 relativistic density functional, the parameters that determine the collective Hamiltonian (mass parameters, moments of inertia, and zero-point energy corrections) are calculated as functions of the deformations β and γ. The diagonalization of the resulting Hamiltonian yields the excitation energies and collective wave functions. An important feature of the model is that physical observables, such as $E2$ transition rates, are calculated in the full configuration space. Using the bare value of the proton charge, parameter-free transition probabilities between eigenstates of the collective Hamiltonian can be directly compared with experimental values. In the current implementation of the model the moments of inertia are calculated with the Inglis-Belyaev formula. The resulting values are considerably smaller than than the empirical moments of inertia and therefore, to compare the relative excitation energies with data, it was necessary to increase the Inglis-Belyaev moments of inertia. The effective values were adjusted to reproduce the experimental energies of the 2_1^+ state in the ground-state band of each nucleus.

A detailed analysis of shape transitions in Nd isotopes has been carried out, from the spherical ^{144}Nd to the strongly deformed ^{154}Nd. With increasing neutron number the Nd isotopes remain prolate deformed in the lowest state, and the calculation reproduces the characteristic signatures of shape transitions: $R_{4/2} \equiv E(4_1^+)/E(2_1^+)$ and

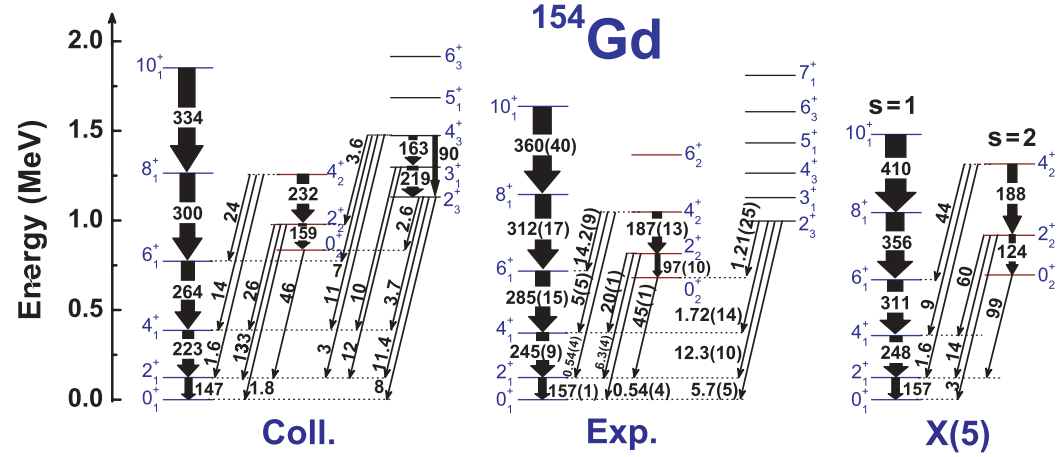

FIG. 13. (Color online) Same as described in the caption to Fig. 12 but for the nucleus ^{154}Gd.

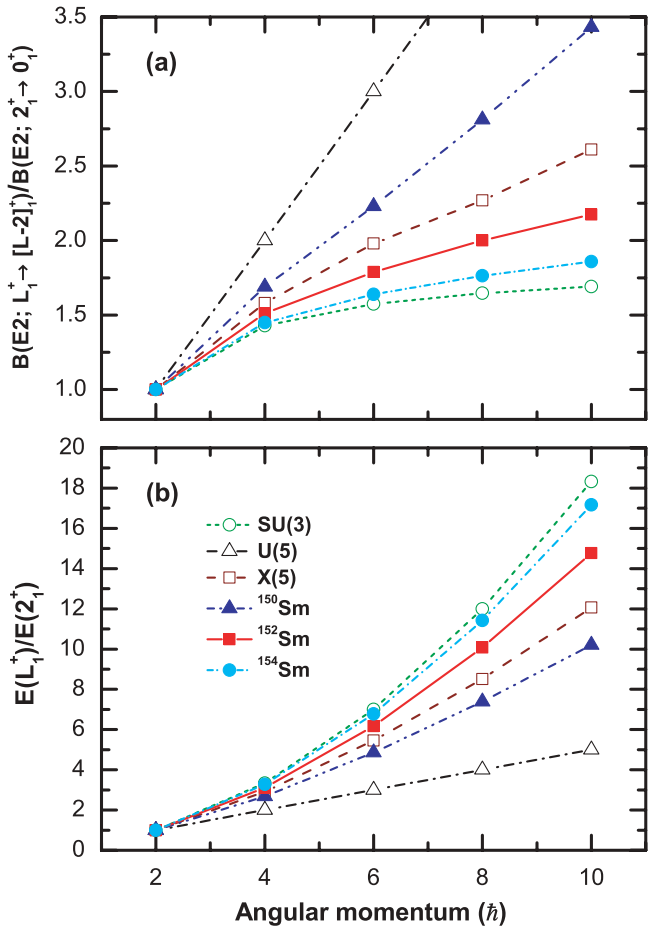

FIG. 14. (Color online) Same as described in the caption to Fig. 7 but for the isotopes ^{150,152,154}Sm.

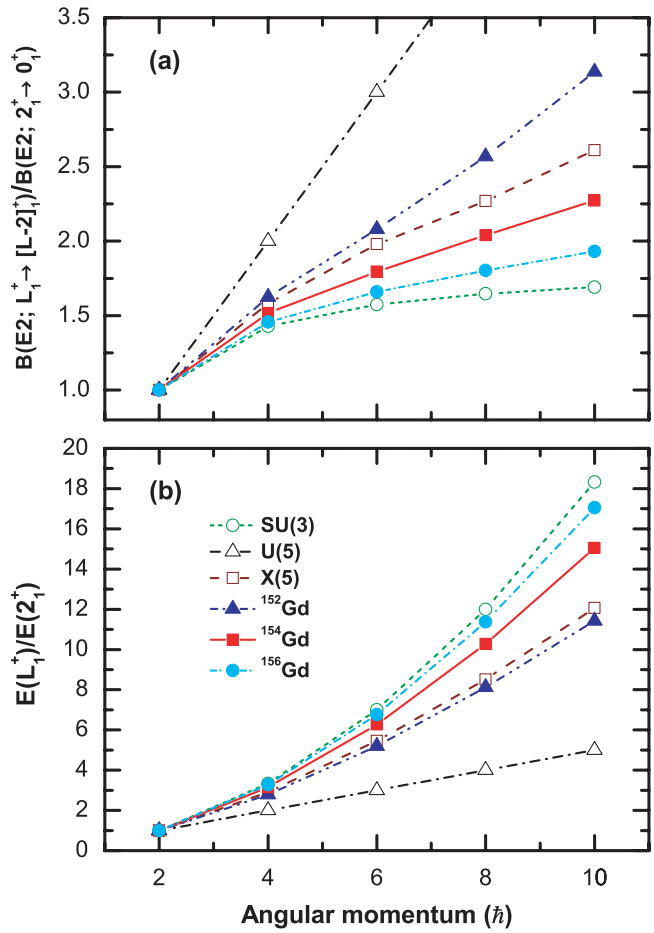

FIG. 15. (Color online) Same as described in the caption to Fig. 7 but for the isotopes ^{152,154,156}Gd.

$B(E2; 2_1^+ \rightarrow 0_1^+)$, as well as the isotopic dependence of the effective order parameter $E(6_1^+)/E(0_2^+)$, which takes the special value of $\approx$1 close to a first-order phase transition point.

Both the data and the results of microscopic calculations show that there is an abrupt change of structure at $N = 90$. The microscopic potential energy surface of ^{150}Nd displays a flat prolate minimum that extends in the interval $0.2 \leqslant \beta \leqslant 0.4$ of the axial deformation parameter, and a parabolic dependence on γ for $\gamma \leqslant 30^\circ$ in the region of the flat prolate minimum. The resulting excitation spectrum of ^{150}Nd, calculated with the PC-F1 density functional, and the corresponding intraband and interband $B(E2)$ values, are in good agreement with available data for the ground-state band and β and γ bands. The calculation reproduces the excitation energies of the bandheads 0_2^+ and 2_3^+ of the β and γ bands, respectively, and, when the Inglis-Belyaev effective moments of inertia are renormalized to the empirical value, also the relative excitation energies in all three bands. The parameter-free predictions for the $B(E2)$'s reproduce the experimental values not only for intraband transitions within the ground-state band and the β band but also for transitions from the β and γ bands to the ground-state band, including the measured branching ratios. The sequence of neutron single-particle levels in Nd isotopes, as functions of the axial deformation parameter β, and the isotopic dependence of the corresponding Fermi level offer a qualitative explanation of the β softness of the potential in ^{150}Nd. Similar results have been obtained for the Sm and Gd nuclei, and in particular the spectra of the collective Hamiltonian and the corresponding $E2$ transition rates reproduce the data in the $N = 90$ isotones ^{152}Sm and ^{154}Gd.

A number of experimental studies over the past decade have disclosed candidate nuclei for quantum shape phase transitions in several mass regions. In addition to geometric and algebraic theoretical methods, it is also important to study these phenomena using microscopic models that explicitly take into account nucleonic degrees of freedom. Among the microscopic approaches to the nuclear many-body problem, the framework of nuclear EDFs provides the most complete description of ground-state properties and collective excitations over the whole nuclide chart. This work, together with similar recent studies, has shown that self-consistent mean-field models based on the EDF framework describe not only general features of shape transitions but also particular properties of spectra and transition rates at the critical point of QPT. However, to calculate excitation spectra and transition probabilities, the self-consistent mean-field approach must be extended to include correlations related to restoration of broken symmetries and fluctuations of collective

variables. This can be done either by performing GCM configuration mixing calculations of projected wave functions or by constructing collective Bohr-type Hamiltonians with deformation-dependent parameters determined from self-consistent mean-field calculations. The possibility to perform self-consistent microscopic studies of shape transitions opens a new perspective on the origin of nuclear QPT in various mass regions. It is therefore important to systematically analyze, also employing different energy-density functionals, various types of shape phase transitions that have been predicted in several regions of medium-heavy and heavy nuclei.

ACKNOWLEDGMENTS

We thank D. Bonatsos and R. F. Casten for useful discussions. This work was supported in part by MZOS project 1191005-1010; by the Major State 973 Program 2007CB815000; the NSFC under Grant Nos. 10435010, 10775004, and 10221003; and by the DFG cluster of excellence "Origin and Structure of the Universe" (www.universe-cluster.de). Z. P. Li acknowledges support from the Croatian National Foundation for Science. The work of J.M., T.N., and D.V. was supported in part by the Chinese-Croatian project "Nuclear structure far from stability."

[1] A. E. L. Dieperink, O. Scholten, and F. Iachello, Phys. Rev. Lett. **44**, 1747 (1980).
[2] D. H. Feng, R. Gilmore, and S. R. Deans, Phys. Rev. C **23**, 1254 (1981).
[3] F. Iachello, N. V. Zamfir, and R. F. Casten, Phys. Rev. Lett. **81**, 1191 (1998).
[4] J. Jolie and R. F. Casten, Nucl. Phys. News Int. **15**, 20 (2005).
[5] R. F. Casten, Nature Physics **2**, 811 (2006).
[6] R. F. Casten and E. A. McCutchan, J. Phys. G: Nucl. Part. Phys. **34**, R285 (2007).
[7] P. Cejnar and J. Jolie, Prog. Part. Nucl. Phys. **62**, 210 (2009).
[8] D. Bonatsos, arXiv:0807.4492v1 [nucl-th].
[9] F. Iachello and N. V. Zamfir, Phys. Rev. Lett. **92**, 212501 (2004).
[10] J. N. Ginocchio and M. W. Kirson, Phys. Rev. Lett. **44**, 1744 (1980).
[11] A. E. L. Dieperink, O. Scholten, and F. Iachello, Phys. Rev. Lett. **44**, 1747 (1980).
[12] F. Iachello, Phys. Rev. Lett. **85**, 3580 (2000).
[13] R. F. Casten and N. V. Zamfir, Phys. Rev. Lett. **85**, 3584 (2000).
[14] F. Iachello, Phys. Rev. Lett. **87**, 052502 (2001).
[15] R. F. Casten and N. V. Zamfir, Phys. Rev. Lett. **87**, 052503 (2001).
[16] J. Meng, W. Zhang, S. G. Zhou, H. Toki, and L. S. Geng, Eur. Phys. J. A **25**, 23 (2005).
[17] Z.-Q. Sheng and J.-Y. Guo, Mod. Phys. Lett. A **20**, 2711 (2005).
[18] R. Fossion, D. Bonatsos, and G. A. Lalazissis, Phys. Rev. C **73**, 044310 (2006).
[19] R. Rodríguez-Guzmán and P. Sarriguren, Phys. Rev. C **76**, 064303 (2007).
[20] T. R. Rodríguez and J. L. Egido, Phys. Lett. **B663**, 49 (2008).
[21] L. M. Robledo, R. R. Rodríguez-Guzmán, and P. Sarriguren, Phys. Rev. C **78**, 034314 (2008).
[22] T. Nikšić, D. Vretenar, G. A. Lalazissis, and P. Ring, Phys. Rev. Lett. **99**, 092502 (2007).
[23] P. Ring and P. Schuck, *The Nuclear Many-Body Problem* (Springer-Verlag, Berlin, 1980).
[24] T. Bürvenich, D. G. Madland, J. A. Maruhn, and P.-G. Reinhard, Phys. Rev. C **65**, 044308 (2002).
[25] N. Pietralla and O. M. Gorbachenko, Phys. Rev. C **70**, 011304(R) (2004).
[26] M. A. Caprio, Phys. Rev. C **72**, 054323 (2005).
[27] D. Bonatsos, D. Lenis, D. Petrellis, P. A. Terziev, and I. Yigitoglu, Phys. Lett. **B632**, 238 (2006).
[28] M. Bender and P.-H. Heenen, Phys. Rev. C **78**, 024309 (2008).
[29] T. Nikšić, Z. P. Li, D. Vretenar, L. Próchniak, J. Meng, and P. Ring, Phys. Rev. C **79**, 034303 (2009).
[30] L. Próchniak, K. Zajac, K. Pomorski, S. G. Rohoziński, and J. Srebrny, Nucl. Phys. **A648**, 181 (1999).
[31] D. R. Inglis, Phys. Rev. **103**, 1786 (1956).
[32] S. T. Belyaev, Nucl. Phys. **24**, 322 (1961).
[33] M. Girod and B. Grammaticos, Nucl. Phys. **A330**, 40 (1979).
[34] R. Krücken *et al.*, Phys. Rev. Lett. **88**, 232501 (2002).
[35] D. Tonev *et al.*, Phys. Rev. C **69**, 034334 (2004).
[36] R. Bijker, R. F. Casten, N. V. Zamfir, and E. A. McCutchan, Phys. Rev. C **68**, 064304 (2003).
[37] NNDC National Nuclear Data Center, Brookhaven National Laboratory, http://www.nndc.bnl.gov/.
[38] LBNL Isotopes Project Nuclear Data Dissemination home page, retrieved March 11, 2002, from http://ie.lbl.gov/toi.html.
[39] D. Bonatsos, E. A. McCutchan, R. F. Casten, and R. J. Casperson, Phys. Rev. Lett. **100**, 142501 (2008).
[40] J. Libert, M. Girod, and J.-P. Delaroche, Phys. Rev. C **60**, 054301 (1999).
[41] R. M. Clark *et al.*, Phys. Rev. C **67**, 041302(R) (2003).
[42] R. F. Casten, N. V. Zamfir, and R. Krücken, Phys. Rev. C **68**, 059801 (2003).